DIGITAL TWIN–BASED SIMULATION CHAIN FOR RAIL MANUFACTURING: ROLL PASS DESIGN, HEAD HARDENING, AND STRAIGHTENING

Sergey Stebunov[1, *], Igor Alimov[1], Pavel Maltsev[1], Vitaliy Belugin[1], Nikolay Biba[2]

[1]QForm Group FZ LLC, Fujairah-Creative City, P. O. Box 4422 Fujairah, UAE, serg@qform3d.com

[2]Micas Simulations Ltd., 107 Oxford Road, Oxford, UK, nick@qform3d.com

*Correspondence: serg@qform3d.com; Tel.: +971 506624574

Abstract: The work introduces a unified virtual process chain for rail production that combines roll pass design, hot rolling, differential quenching of the rail head, and final straightening within a single simulation route. The first stage is carried out in QKaliber, where analytical models are used to evaluate pass geometry together with the main process variables, including deformation, thermal state, rolling speed, and force–energy characteristics. These fast calculations support selection of feasible pass schedules and allow potentially critical loads on rolls to be identified before detailed numerical analysis.
The verified roll pass design is subsequently imported into QForm UK for finite element simulation of rail rolling. For the heat-treatment stage, boundary conditions generated by a dedicated CFD model are transferred to QForm UK to reproduce differential cooling of the rail head. This coupled methodology captures nonuniform heat exchange, local temperature gradients, and phase transformation kinetics during quenching, while preserving process-specific effects such as air-flow distribution and cooling intensity.
The final stage addresses rail straightening and examines how inherited temperature fields and residual stresses affect the final geometry of the product. Taken together, the proposed framework provides an integrated digital representation of rail manufacturing and demonstrates the value of combining analytical design tools with FEM and CFD models. Such an approach can shorten process development, improve product consistency, and increase the durability of rolls in modern rolling mills.

KEYWORDS: RAIL MANUFACTURING, DIGITAL TWIN, LONG PRODUCT ROLLING, ROLL PASS DESIGN, QUENCHING SIMULATION, RESIDUAL STRESS, STRAIGHTENING, FEM

INTRODUCTION

Rail production is a multi-stage technological process in which the final properties of the product are formed not by a single operation, but by the interaction of rolling, heat treatment, cooling and straightening. For this reason, the development of a new rail profile or the adaptation of an existing process to a different steel grade usually requires a large number of technological assumptions, plant trials and subsequent corrections. A virtual process chain makes it possible to analyze these stages before industrial testing and to evaluate how the parameters selected at one step influence the final geometry, hardness and residual stress state of the rail [1,2].

In this work, a digital model of the production route for a 60E1 rail made of R350HT pearlitic steel in accordance with EN 13674-1 is considered. The proposed workflow combines roll pass design, hot rolling simulation, rail head hardening, cooling on the cooling bed and final straightening. Roll pass design is performed in QKaliber, where the pass sequence and the main rolling parameters are calculated using analytical models. The obtained technological data are then transferred to QForm UK for finite element simulation of rolling and subsequent thermal-mechanical operations.

The main purpose of this integrated approach is to connect the process parameters with the final quality indicators of the rail. The rolling stage determines the geometry and thermal state of the workpiece, the head hardening stage forms the required hardness distribution, while cooling and straightening influence the final residual stress state. Therefore, the complete simulation chain allows the rail manufacturing route to be evaluated not only in terms of forming feasibility, but also in terms of compliance with the required hardness, tensile strength and residual stress limits. EN 13674-1 limits the tensile residual stress at the center of the rail foot to +250 MPa [3].

1. METHODOLOGY

The general structure of the proposed digital process chain is shown in Figure 1. The workflow starts with roll pass design, where the sequence of grooves and the main rolling parameters are defined. The resulting data are then used for finite element simulation of the rolling process. After rolling, the thermal state of the rail is transferred to the head hardening stage, where differential cooling of the rail head is simulated. The following cooling stage describes the temperature evolution of the full rail on the cooling bed. Finally, the straightening simulation is performed in order to evaluate the final geometry and the redistribution of residual stresses. Thus, all main stages of the 60E1 rail manufacturing route are included in a single digital simulation chain.

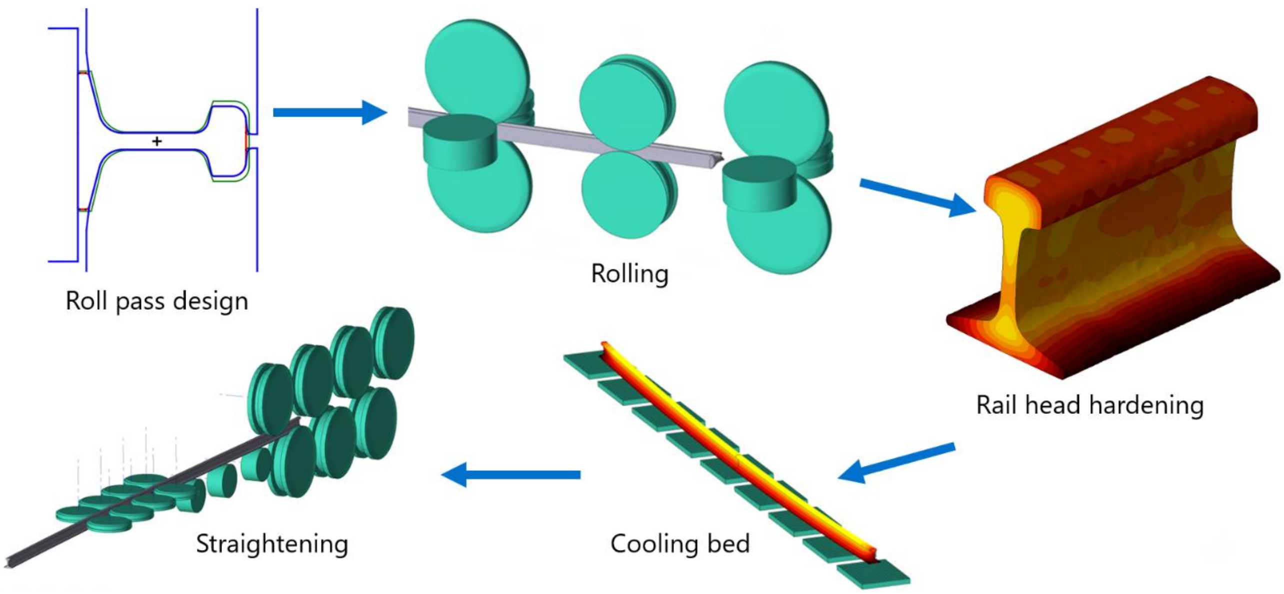

Fig. 1. Digital simulation chain for 60E1 rail manufacturing from roll pass design to rolling, rail head hardening, cooling and straightening, used for virtual assessment of hardness, strength and residual stresses.

1.1 ROLL PASS DESIGN

Roll pass design was used as the first stage of the proposed simulation chain. For the 60E1 rail profile, the pass schedule was prepared in QKaliber using a combination of analytical rolling models and geometric design tools [4,5]. At this stage, the objective was not only to obtain the required final rail section, but also to define a feasible technological route that could be transferred to the subsequent finite element simulation. Two complementary design approaches were applied. The finishing part of the pass schedule was developed using an inverse design procedure, starting from the final rail profile and moving backwards to an intermediate leader profile. This approach is especially useful for complex rail sections, because the head, web and foot regions can be controlled separately during the shape transformation. The breakdown part of the schedule was then designed in the forward direction, from the rectangular billet to the same leader profile. The resulting design strategy is shown in Figure 2.

During the RPD stage, QKaliber was also used to estimate the main rolling parameters, including reduction, spread, elongation, rolling force, torque and temperature evolution. These estimates provided a preliminary check of the pass schedule before detailed FEM simulation.

The roll pass design data obtained in QKaliber were used as the input for the hot rolling simulation in QForm UK [6]. The imported data included groove geometries, roll rotations and the pass sequence. As a result, the FEM rolling model provided the geometry of the rail after the final pass together with the corresponding temperature distribution. This thermal state was then used as the initial condition for the subsequent rail head hardening analysis.

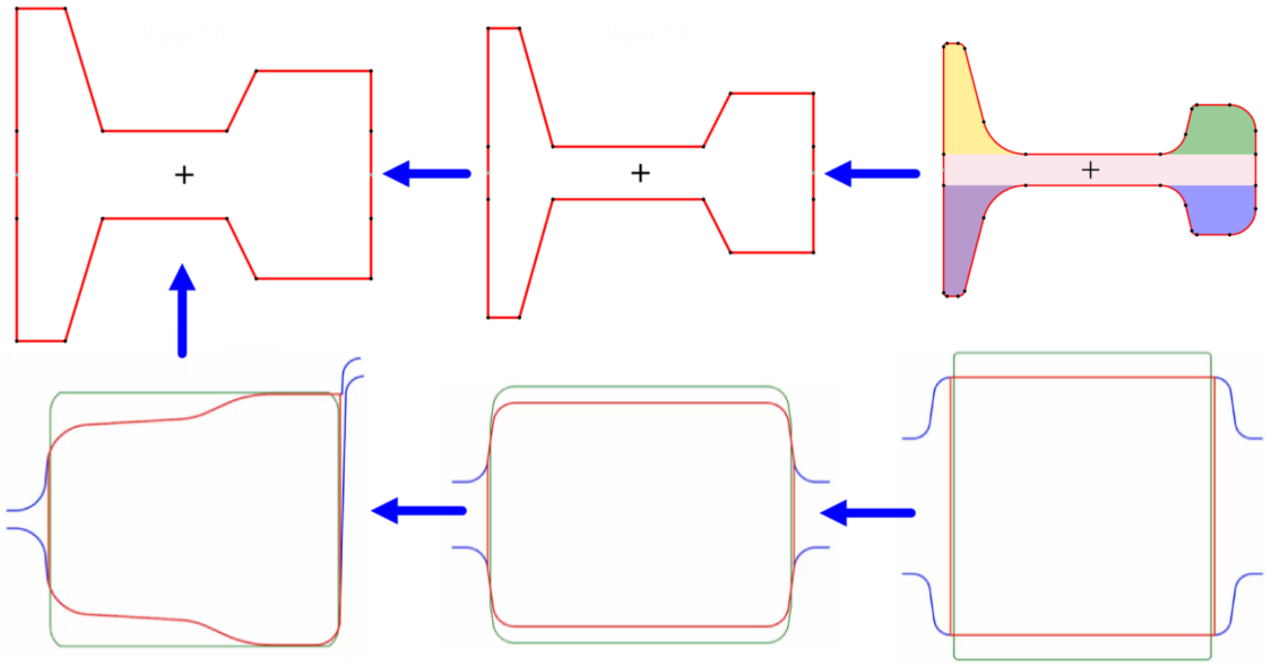

Fig. 2. Roll pass design strategy for the 60E1 rail profile in QKaliber: inverse design from the final rail section to the leader profile and forward design from the rectangular billet to the same leader profile.

1.2 RAIL HEAD HARDENING SIMULATION

After the rolling, the rail undergoes differential head hardening, in which the rail head is intensively cooled to increase hardness, while the web and foot cool at a lower rate. Since the cooling intensity strongly depends on the local air flow and on the position of the surface relative to the cooling nozzles, the heat treatment stage was simulated using a coupled CFD–FEM approach [7]. The CFD model was used to determine the local heat exchange conditions during air cooling, while the FEM model in QForm UK was used to calculate the thermal response, phase transformations and final hardness of the rail.

A CFD model of the rail head quenching unit was developed in ANSYS Fluent using a 300 mm rail segment. The model included a pressure inlet representing the air jet and an outlet at atmospheric pressure. The initial rail temperature was taken from the FEM rolling simulation results. Symmetry boundary conditions were applied at the faces of the segment to represent a long rail. The CFD analysis provided spatially non-uniform and time-dependent heat transfer coefficients on the rail surface, with higher cooling intensity in the regions directly exposed to the air jets and lower cooling intensity in shielded areas (Figure 3).

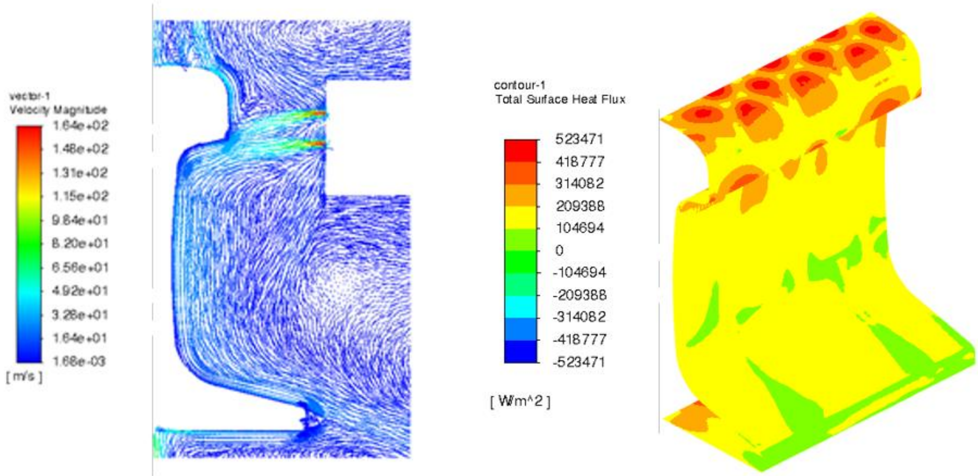

a. b.

Fig. 3. CFD simulation of rail head cooling in ANSYS Fluent: velocity field in the cooling zone and distribution of heat extraction on the rail surface.

To reproduce the non-uniform cooling conditions during rail head hardening, the thermal boundary conditions obtained from the CFD model were transferred to the FEM model as spatially distributed surface data. This approach is necessary because the cooling intensity varies significantly along the rail head perimeter. Therefore, the use of a single averaged heat transfer coefficient for the entire rail surface would not accurately represent the real cooling process.

In the present workflow, the CFD results were imported into QForm UK as surface boundary conditions assigned to the rail surface. Depending on the available CFD output, the boundary condition can be specified either directly as a surface heat flux density or as an environment-type condition including convection and radiation parameters. In the latter case, the convective heat transfer coefficient and emissivity can be defined directly or recalculated from the total heat flux and the radiative heat flux. The total heat flux on the surface can be represented as the sum of convective and radiative components [8]:

$$q_{\Sigma} = q_c + q_R \quad (1)$$

where q_{Σ} is the total heat flux, q_c is the convective heat flux, and q_R is the radiative heat flux. The convective component is expressed as:

$$q_c = \alpha_c (T_s - T_{\infty}) \quad (2)$$

and the radiative component as:

$$q_R = \varepsilon\sigma(T_s^4 - T_\infty^4) \quad (3)$$

where α_c is the convective heat transfer coefficient, T_s is the rail surface temperature, T_∞ is the ambient temperature, ε is the emissivity, and σ is the Stefan–Boltzmann constant. If the total and radiative heat fluxes are known from the CFD solution, the corresponding convection coefficient and emissivity can be evaluated as:

$$\alpha_c = \frac{q_\Sigma - q_R}{T_s - T_\infty}; \ \varepsilon = \frac{q_R}{\sigma(T_s^4 - T_\infty^4)} \quad (4)$$

This conversion makes it possible to use CFD-calculated local heat exchange conditions in the thermal-mechanical FEM simulation. In addition, periodic mapping of the imported surface data can be applied along the rail length, which is especially useful when a short CFD model of the cooling zone is used to represent repeated cooling units acting on a full-length rail. In this study, the cooling conditions obtained for the 300 mm CFD segment were applied periodically to a 12 m rail model in QForm UK. This allowed the thermal and metallurgical response of the full rail to be simulated while preserving the local cooling intensity generated by the head hardening equipment.

During the FEM simulation of rail head hardening, the imported heat transfer coefficients controlled the local cooling rate of the rail surface. As the rail cooled from the austenitization temperature, the phase transformation model predicted the formation of pearlite in the rail head. The objective of this stage was to verify that the selected cooling conditions provide the required hardness level while avoiding the formation of brittle phases such as martensite. The resulting temperature history was also retained for the subsequent residual stress analysis and straightening simulation [9,10].

1.3 STRAIGHTENING SIMULATION

After rail head hardening and cooling on the cooling bed, the rail was transferred to the straightening simulation. At this stage, the FEM model contained the temperature field and residual stress state inherited from the previous thermal treatment steps. This is important because the straightening operation does not only correct the final rail geometry, but also modifies the internal stress distribution formed during differential cooling [11,12].

The straightening process was modeled in QForm UK using a multi-roll straightening machine with horizontal and vertical roll groups (Figure 4). The horizontal rolls were used to correct vertical curvature of the rail, while the vertical rolls were applied to reduce lateral deviations. The rail was passed through the roll system, and the resulting deformation was calculated together with the redistribution of longitudinal residual stresses.

The objective of this stage was to evaluate the final state of the rail after the complete manufacturing route. Therefore, the straightening simulation was used not only as a geometric correction step, but also as the final verification stage for residual stresses. The obtained stress distribution after straightening was subsequently compared with the allowable stress limits for head-hardened rails.

Fig. 4. FEM model of rail straightening in QForm UK using horizontal and vertical roll groups. The simulation accounts for correction of rail curvature and redistribution of residual stresses after head hardening and cooling.

2. RESULTS

2.1 VERIFICATION OF RAIL HEAD HARDNESS AFTER QUENCHING

The phase transformation results showed that the rail head transformed predominantly into pearlite, while no martensite was predicted under the selected quenching conditions. This is a desirable outcome, since martensite is a brittle phase that may reduce rail durability under service loading [10]. The hardness distribution obtained after rail head quenching was evaluated against the EN 13674-1 requirements [3], as shown in Figure 5. The simulated hardness at the running surface was 367.9 HBW, which falls within the required range of 350–390 HBW. At the remaining control points, the predicted hardness values were 333.8–336.5 HBW in the hardened layer and corner regions, and 312.6 HBW in the head center, all satisfying the corresponding minimum EN 13674-1 limits. Thus, the simulation confirms that the selected quenching conditions provide the required hardness level across the rail head without exceeding the upper limit at the running surface. These results demonstrate how the proposed simulation chain can be used for virtual verification of the heat-treatment stage before production trials.

In addition to hardness prediction, the quenching simulation provides the temperature history required for the subsequent residual stress analysis. The non-uniform cooling of the rail head produces temperature gradients that influence the formation of residual stresses and must therefore be transferred to the following straightening simulation.

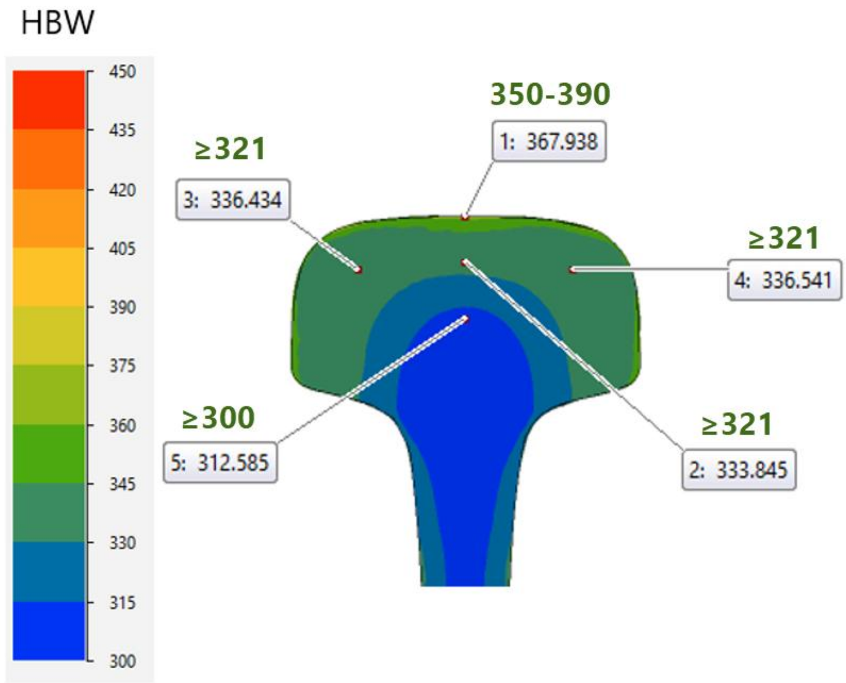

Fig. 5. Distribution of Brinell hardness (HBW) in the rail head after quenching. The green labels indicate the EN 13674-1 hardness requirements, while the callouts show the simulated HBW values.

The hardness distribution obtained after rail head quenching was evaluated against the EN 13674-1 requirements [3], as shown in Figure 5. The simulated hardness at the running surface was 367.9 HBW, which falls within the required range of 350–390 HBW. At the remaining control points, the predicted hardness values were 333.8–336.5 HBW in the hardened layer and corner regions, and 312.6 HBW in the head center, all satisfying the corresponding minimum EN 13674-1 limits. Thus, the simulation confirms that the selected quenching conditions provide the required hardness level across the rail head without exceeding the upper limit at the running surface. These results demonstrate how the proposed simulation chain can be used for virtual verification of the heat-treatment stage before production trials.

In addition to hardness prediction, the quenching simulation provides the temperature history required for the subsequent residual stress analysis. The non-uniform cooling of the rail head produces temperature gradients that influence the formation of residual stresses and must therefore be transferred to the following straightening simulation.

2.2 VERIFICATION OF THE FINAL RESIDUAL STRESS STATE AFTER STRAIGHTENING

The residual stress state of the rail was evaluated before and after the final straightening operation. The stresses formed during differential cooling are inherited by the rail and are subsequently redistributed due to the additional plastic deformation introduced during roller straightening. Therefore, straightening influences not only the final rail geometry but also its internal stress state [11-13]. Fig. 6 shows the distribution of longitudinal residual stresses along the selected evaluation path in the rail head. Before straightening, the stresses in most of the evaluated region are compressive, with values of approximately −80 MPa near the running surface. After straightening, the stress distribution changes substantially and a broad tensile region develops in the central part of the rail head, reaching approximately +240 MPa. This demonstrates the significant influence of the straightening operation on the residual stresses inherited from the preceding cooling stages.

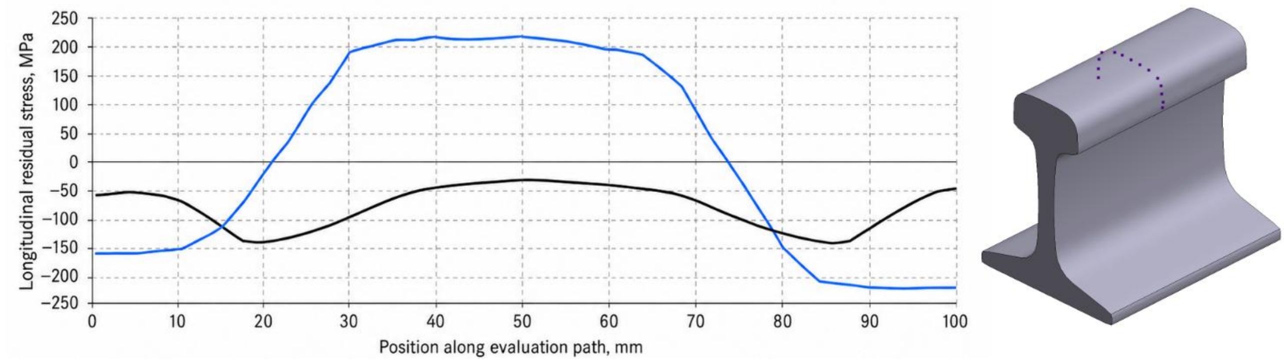

Fig. 6. Distribution of longitudinal residual stresses before and after straightening: rail head. The black and blue curves correspond to the stress state before and after straightening, respectively. The green dashed line in (b) indicates the EN 13674-1 residual tensile stress limit of +250 MPa at the center of the rail foot.

The corresponding stress distribution in the rail foot is shown in Figure 7. Before straightening, the central region of the foot is characterized by relatively low residual stresses, while the outer regions are predominantly in compression. After straightening, tensile stresses develop in the central part of the foot and reach approximately +200 MPa, whereas the outer regions remain under compression.

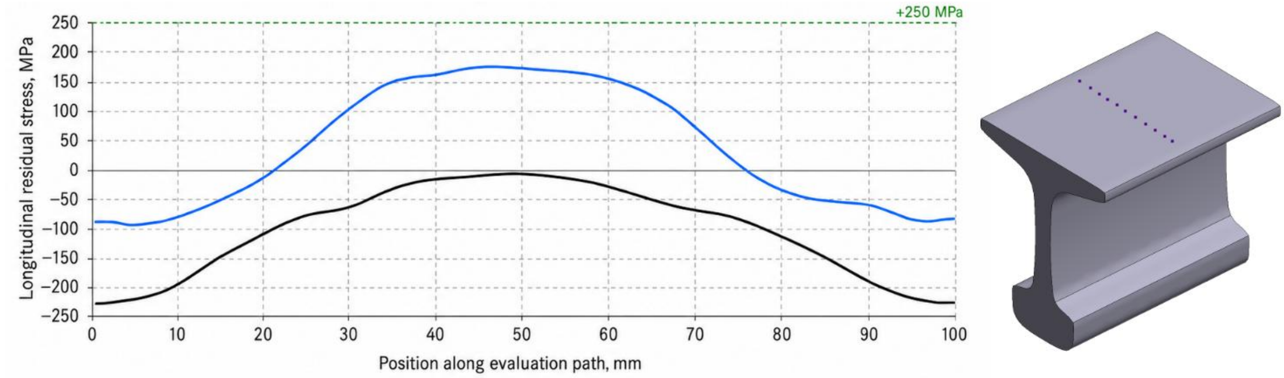

Fig. 7. Distribution of longitudinal residual stresses before and after straightening: rail foot. The black and blue curves correspond to the stress state before and after straightening, respectively. The green dashed line indicates the EN 13674-1 residual tensile stress limit of +250 MPa at the center of the rail foot.

The residual tensile stress at the center of the rail foot is one of the criteria specified by EN 13674-1 [3]. The calculated value after straightening remains below the allowable limit of +250 MPa, indicated by the green dashed line in Figure 7. Thus, the simulation makes it possible to evaluate not only the redistribution of stresses during straightening, but also the compliance of the final residual stress state with the specified requirement before production trials.

In the rail web, the longitudinal residual stress also becomes more compressive after straightening, changing from approximately −40 MPa to −180 MPa. Overall, the results show that straightening causes a substantial redistribution of residual stresses throughout the rail cross-section, while the final stress level at the critical control location in the rail foot remains within the allowable limit.

3. DISCUSSION AND CONCLUSION

The proposed simulation chain was used to evaluate the complete manufacturing route of a 60E1 rail made of R350HT steel, from roll pass design and hot rolling to head hardening, cooling and final straightening. The results show that the selected process parameters provide the required final properties of the rail.

The calculated hardness distribution satisfies the EN 13674-1 requirements, with approximately 368 HBW at the running surface and the required hardness maintained at all evaluated locations in the rail head. The predicted ultimate tensile strength is not lower than 1200 MPa. After straightening, the tensile residual stress at the center of the rail foot reaches approximately +200 MPa and remains below the allowable limit of +250 MPa [3,14].

The results also demonstrate the importance of considering the manufacturing stages as a connected process chain, since the thermal history generated during rolling and cooling directly influences phase transformations and the residual stress state after straightening. The proposed workflow therefore provides a practical tool for virtual verification and adjustment of rail manufacturing technology before production trials.

Future work will focus on extending the methodology to other long products and on improving the prediction of microstructural and mechanical properties, including grain size and strength characteristics [15].

REFERENCES

[1] Kritzinger W, Karner M, Traar G, Henjes J, Sihn W. Digital Twin in manufacturing: a categorical literature review and classification. IFAC-PapersOnLine. 2018;51(11):1016-1022. doi:10.1016/j.ifacol.2018.08.474.

[2] Milenin A, Zalecki W, Pernach M, Rauch Ł, Kuziak R, Zygmunt T, et al. Numerical simulation of manufacturing process chain for pearlitic and bainitic steel rails. Arch Civ Mech Eng. 2020;20:107. doi:10.1007/s43452-020-00107-0.

[3] European Committee for Standardization (CEN). EN 13674-1:2011+A1:2017. Railway applications - Track - Rail - Part 1: Vignole railway rails 46 kg/m and above. Brussels: CEN; 2017.

[4] Bahtinov BP, Shternov MM. Roll pass design. Moscow: Metallurgizdat; 1953. 783 p.

[5] Wusatowski Z. Grundlagen des Walzens. Leipzig: VEB Deutscher Verlag für Grundstoffindustrie; 1963. 691 p.

[6] Biba N, Stebunov S, Maltsev P, Belugin V, Alimov I. Integration of automated roll pass design and simulation for the development of shape rolling technology. Materials Research Proceedings. 2024;44:758-767. doi:10.21741/9781644903254-81.

[7] Ferro L. idRHa+ProMod - Rail Hardening Control System. IOP Conf Ser Mater Sci Eng. 2016;119:012006. doi:10.1088/1757-899X/119/1/012006.

[8] Bergman TL, Lavine AS, Incropera FP, DeWitt DP. Fundamentals of heat and mass transfer. 8th ed. New York: Wiley; 2017.

[9] Kuziak R, Pidvysots'kyy V, Pernach M, Rauch Ł, Zygmunt T, Pietrzyk M. Selection of the best phase transformation model for optimization of manufacturing processes of pearlitic steel rails. Arch Civ Mech Eng. 2019;19(2):535-546. doi:10.1016/j.acme.2018.12.004.

[10] Jabłońska M, Lewandowski F, Chmiela B, Gronostajski Z. Advanced heat treatment of pearlitic rail steel. Materials (Basel). 2023;16(19):6430. doi:10.3390/ma16196430.

[11] Schleinzer G, Fischer FD. Residual stress formation during the roller straightening of railway rails. Int J Mech Sci. 2001;43(10):2281-2295. doi:10.1016/S0020-7403(01)00041-8.

[12] Betegón Biempica C, del Coz Díaz JJ, García Nieto PJ, Peñuelas Sánchez I. Nonlinear analysis of residual stresses in a rail manufacturing process by FEM. Appl Math Model. 2009;33(1):34-53. doi:10.1016/j.apm.2007.10.015.

[13] Kaiser R, Stefenelli M, Hatzenbichler T, Antretter T, Hofmann M, Keckes J, et al. Experimental characterization and modelling of triaxial residual stresses in straightened railway rails. J Strain Anal Eng Des. 2015;50(3):190-198. doi:10.1177/0309324714560040.

[14] Żak S. Quality assessment of heat-treated rails in the R350HT grade. Mater Sci Pol. 2025;43(4):59-78. doi:10.2478/msp-2025-0042.

[15] Tretyakov D, Biba N, Belugin V, Gartvig A, Shitikov A, Stebunov S. An AI-based approach to developing a microstructural model for multi-stage hot deformation processes. Key Eng Mater. 2026;1050:183-192. doi:10.4028/p-dWx8G5.